Development of a ^{124}I-labeled version of the anti-PSMA monoclonal antibody capromab for immunoPET staging of prostate cancer: Aspects of labeling chemistry and biodistribution

VLADIMIR TOLMACHEV[1], JENNIE MALMBERG[2], SERGIO ESTRADA[2], OLOF ERIKSSON[2] and ANNA ORLOVA[2]

[1]Division of Biomedical Radiation Sciences, Rudbeck Laboratory, [2]Preclinical PET Platform, Uppsala University, Uppsala, Sweden

Received January 8, 2014; Accepted February 24, 2014

DOI: 10.3892/ijo.2014.2376

Abstract. Correct staging of prostate cancer is an unmet clinical need. Radionuclide targeting of prostate-specific membrane antigen (PSMA) with ^{111}In-labeled capromab pendetide (ProstaScint) is a clinical option for prostate cancer staging. We propose the use of ^{124}I-labeled capromab to decrease the retention of radioactivity in healthy organs (due to the non-residualizing properties of the radiolabel). The use of ^{124}I as a label should increase imaging sensitivity due to the advantages of PET as an imaging modality. Capromab targets the intracellular domain of PSMA; accumulation of radioactivity in the tumor should not depend on internalization of the antigen/antibody complex. Capromab was iodinated, and its targeting properties were compared with indium labeled counterpart in LNCaP xenografts in dual isotope mode. PSMA-negative xenografts (PC3) were used as a negative control. Radioiodinated capromab bound to PSMA specifically. Biodistribution of ^{125}I/^{111}In-capromab showed a more rapid clearance of iodine radioactivity from liver, spleen, kidneys, bones, colon tissue, as well as tumors. Maximum tumor uptake (13±8% ID/g for iodine and 29±9% ID/g for indium) and tumor-to-non-tumor ratios for both agents were measured 5 days post-injection (pi). High tumor accumulation and low uptake of radioactivity in normal organs were confirmed using microPET/CT 5 days pi of ^{124}I-capromab.

Correspondence to: Dr Anna Orlova, Preclinical PET Platform, Uppsala University, Dag Hammarskjöldsv 14C, 3 tr, 751 83 Uppsala, Sweden
E-mail: anna.orlova@pet.medchem.uu.se

Abbreviations: PSMA, prostate-specific membrane antigen

Key words: prostate cancer, iodine-124, PET, molecular imaging, prostate-specific membrane antigen

Introduction

Correct staging of prostate cancer is an unmet clinical need. Conventional anatomical imaging modalities (CT and MRI) tend to understage prostate cancer due to poor sensitivity to soft tissue metastases. Currently, a significant number of patients with extraprostatic disease undergo non-curative surgery due to false negative diagnoses (1). The utility of PET or PET/CT using ^{18}F-FDG is limited in this arena; prostate cancer glucose utilization is low, and FDG uptake is insufficient in up to 81% of primary prostate cancers (2,3). Other metabolic PET tracers, such as ^{11}C- or ^{18}F-labeled choline or ^{11}C-acetate, have shown some promising results in the clinic. However, elevated radiolabeled choline uptake was detected not only in malignant but also in hyperplastic prostate tissues. Histological evaluation suggests an alarmingly high false-positive rate for ^{11}C-choline (4). Sensitivity of ^{11}C-acetate-based PET is suboptimal in patients with low PSA values (5). Thus, accurate staging of prostate cancer using PET appears to require more research and development.

An alternative approach to visualization of prostate cancer is radionuclide targeting of antigens expressed in prostate cancer cells, e.g. 'free' prostate specific antigen, fPSA (6), prostate stem cell antigen, PSCA (7) or prostate specific membrane antigen, PSMA (8). Recently it was shown in a preclinical study (9) that radiolabeled monoclonal antibody (mAb) 5A10 recognizing an epitope adjacent to the catalytic cleft of PSA, can selectively target fPSA in androgen receptor positive xenografts. However, decrease of androgen receptor expression in castrate refractory patients could be a challenge in clinical setting.

Expression of PSMA is low in normal prostate tissue, but it increases in prostate cancer and is significantly upregulated as tumors dedifferentiate into higher grade, androgen-resistant and metastatic lesions (10). Recently, it was proposed that PSMA over-expression on circulating cancer cells could serve as a biomarker in castration resistance prostate cancers (11). High-affinity small-molecule inhibitors of PSMA labeled with $^{123/131}$I and ^{99m}Tc for SPECT and with ^{68}Ga for PET imaging modalities demonstrated high accumulation in small metastases in men and are under evaluation in international clinical trials (12). Currently, PSMA is used to image prostate cancer via ^{111}In-labeled capromab pendetide (ProstaScint), which is approved for clinical use in the

United States. In a pivotal study, ProstaScint demonstrated better sensitivity (63%) in detection of lymph node metastases than CT (4%) or MRI (15%) (13). The use of SPECT/CT for imaging increased the sensitivity of ^{111}In-capromab pendetide further. Nonetheless, further improving the sensitivity of prostate cancer imaging is desirable (10).

A possible way to increase the sensitivity of radionuclide imaging using monoclonal antibodies is the use of PET instead of SPECT (14). PET provides better resolution (and, accordingly, lower influence of partial volume effect) and better registration efficiency, which improves imaging quality. Feasibility of antibody-mediated PET imaging (immunoPET) has been demonstrated in a number of preclinical studies using monoclonal antibodies targeting several tumor-associated antigens (6,15-20). Preliminary clinical data concerning immunoPET imaging of HER2-expressing breast cancer (21) and renal cell carcinoma (22) are very encouraging. This gives good support to the hypothesis that the use of PET in combination with capromab labeled with an appropriate positron-emitting label would improve the sensitivity of PSMA imaging and therefore the quality of prostate cancer staging.

Clearance of intact monoclonal antibodies from the circulation is relatively slow. To provide sufficient clearance and increase contrast, imaging is usually performed four to five days after the injection of ^{111}In-capromab (10). A positron-emitting radionuclide with a sufficient half-life is required as a label for capromab. Two nuclides, ^{89}Zr (half-life 78.4 h) and ^{124}I (half-life 100.3 h), are potential options. It has been shown that ^{89}Zr (as a radiometal) is most suitable for monoclonal antibodies that are internalized upon binding to their antigens. After internalization of an antibody and its degradation in lysosomes, ^{89}Zr is trapped intracellularly, e.g., Perk *et al* (17). This increases the retention of radioactivity by the tumor(s). A downside of this property is that ^{89}Zr is efficiently retained by healthy organs that catabolize antibodies, mainly liver and spleen (17). In addition to this, there is an appreciable accumulation of ^{89}Zr in bone (17,21). Indeed, labeling with ^{89}Zr of two anti-PSMA monoclonal antibodies (mAbs) targeting the intra- (7E11, capromab) and extra- (J591) cellular domains of PSMA was recently reported (24,32). In a murine xenograft model, both mAbs demonstrated high and specific tumor uptake (up to 40% ID/g at 4 days pi) but also high liver, spleen and bone uptake. The radiocatabolites of ^{124}I-labeled internalized antibodies 'leak' from cancer cells after internalization, which reduces tumor accumulation of radioiodine in comparison with radiometals. However, the retention of ^{124}I radioactivity in liver, spleen and bones is lower than that of ^{89}Zr (17).

Capromab binds to an intracellular portion of PSMA (25). In fact, the antibody works by targeting necrotic cells in the tumors and does not undergo internalization and proteolytic lysosomal degradation after binding. We hypothesized that the use of ^{124}I would be possible for capromab-mediated immunoPET because tumor retention should not be dependent on residualizing properties of a radiometal label but accumulation in normal tissues might be lower for radioiodine.

The goals of the study were to select a method for radioiodination that preserves the specificity of binding to PSMA after labeling and to test whether the use of radioiodine reduces the uptake of radioactivity in healthy organs in comparison with the use of radiometals.

Two approaches (Fig. 1) to the radioiodination of capromab were selected: direct iodination using chloramine-T and indirect radioiodination using *N*-succinimidyl-*p*-(trimethylstannyl)-benzoate.

Direct radioiodination using chloramine-T was evaluated because it is a simple and robust method. However, the use of chloramine-T may destroy the binding specificity of some antibodies due to iodination of tyrosines in the binding site or by disruption of critical disulfide bonds in an antibody (26). For this reason, a milder indirect radioiodination using *N*-succinimidyl-*p*-(trimethylstannyl)-benzoate was evaluated as an alternative. The iodine isotope ^{125}I (half-life 60 days) was used *in vitro* and in biodistribution studies as a convenient surrogate for ^{124}I (half-life 78.4 h).

Materials and methods

Materials. The monoclonal antibody capromab pendetide (ProstaScint®) was kindly provided by EUSA Pharma as a commercial kit (0.5 mg/ml, PBS, pH 6.0). *N*-succinimidyl-*p*-(trimethylstannyl)-benzoate has been synthesized in our laboratories according to the method described by Koziorowski *et al* (27). Chloramine-T and sodium metabisulfite were from Sigma-Aldrich (St. Louis, MO).

Buffers, such as 0.1 M phosphate-buffered saline (PBS), pH 7.5, and 0.07 M sodium borate, pH 9.3, were prepared using common methods from chemicals supplied by Merck (Darmstadt, Germany). High-quality Milli-Q water (resistance higher than 18 MΩ cm) was used for preparing solutions. [^{111}In]-indium chloride was purchased from Covidien (Mansfield, MA), [^{125}I]-sodium iodide from Perkin-Elmer (Waltham, MA), and [^{124}I]-sodium iodide from IBA Molecular (Albany, NY). NAP-5 size-exclusion columns were from GE Healthcare (Little Chalfont, UK).

The radioactivity was measured using an automated gamma-counter with a 3-inch NaI(Tl) detector (1480 Wizard; Wallac Oy, Turku, Finland). In the dual-isotope biodistribution experiments, ^{125}I radioactivity was measured in the energy window from 6 to 60 keV, and ^{111}In was measured from 100 to 450 keV. The data were corrected for dead time, spill over and background. Evaluation of purity was performed using 150-771 Dark Green Tec-Control Chromatography strips (Biodex Medical Systems, Shirley, NY), and distribution of radioactivity along the ITLC strips was measured on a Cyclone™ Storage Phosphor System (further referred to as Phosphor Imager) and analyzed using the OptiQuant™ image analysis software. MicroPET-CT and microSPECT-CT studies were performed in a Triumph™ Trimodality system (GammaMedica Inc, Salem, NH), an integrated SPECT/PET/CT platform optimized for small animals in pre-clinical applications. Image co-registration and analysis was performed in PMOD v3.13 (PMOD Technologies Ltd, Zurich, Switzerland).

The PSMA-expressing cell line LNCaP (prostate cancer lymph node metastasis) and PSMA-negative cell line PC3 (prostate cancer bone metastasis), both from ATCC (LGC Promochem, Borås, Sweden), were used in this study. Cells were cultured in RPMI medium (Flow Irvine, Lake Forest, CA). The medium was supplemented with 10% fetal calf serum (Sigma-Aldrich), 2 mM L-glutamine and PEST (100 IU/ml

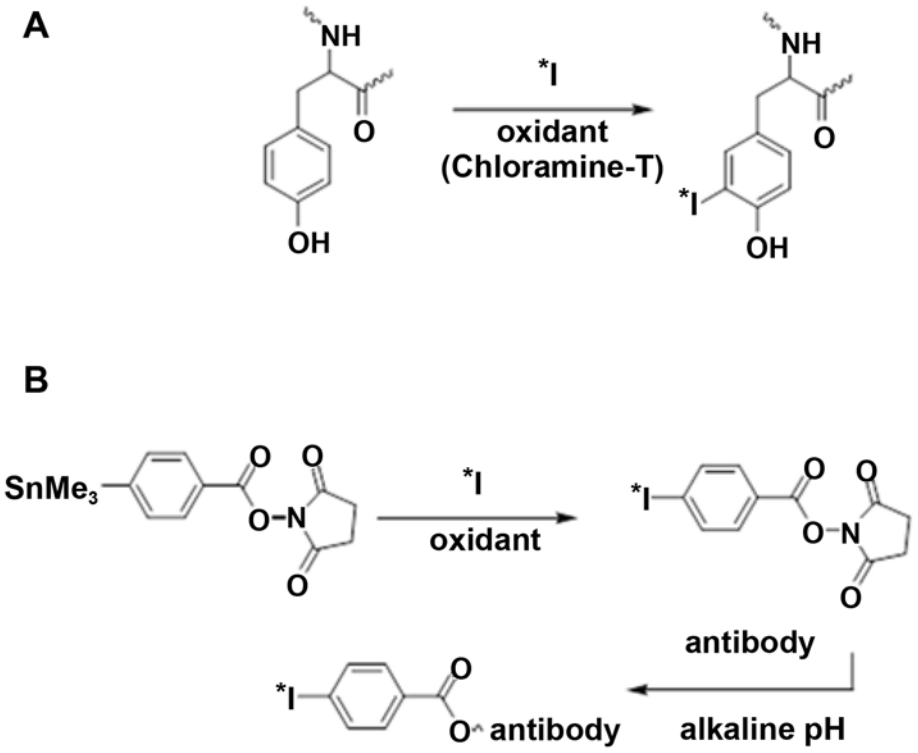

Figure 1. Approaches to the radioiodination of capromab tested in this study. (A) Direct radioiodination using chloramine-T. Radioiodine is *in situ* oxidized and binds to activated phenolic rings in the tyrosine residues of an antibody. (B) Indirect radioiodination using *N*-succinimidyl-*p*-(trimethylstannyl)-benzoate. After radioiodination of the precursor, succinimidyl-*p*-iodobenzoate binds to the lysine residues of an antibody. The antibody is not exposed to an oxidant in this method.

penicillin and 100 μg/ml streptomycin), all from Biokrom AG (Berlin, Germany). For the LNCaP cell line, media was additionally supplemented with Na-pyruvate and HEPES (Biokrom AG).

Labeling chemistry. Labeling of capromab pendetide with ^{111}In was performed according to the manufacturer's instructions. The purity of the conjugate (designated as ^{111}In-capromab) was determined using ITLC.

For indirect radioiodination, the buffer provided in the commercial kit was changed to 0.07 M sodium borate, pH 9.3, by ultrafiltration using Centricon 30. For labeling, ^{125}I solution (6 μl, 15 MBq) was diluted with 10 μl 0.1% acetic acid/water. A solution of *N*-succinimidyl-*p*-(trimethylstannyl)-benzoate (5 μl, 1 mg/ml in 5% acetic acid/methanol) was added, and the reaction was initiated by adding 10 μl of chloramine-T solution (4 mg/ml in water). After 5 min of incubation at room temperature, the reaction was quenched by the addition of sodium metabisulfite (10 μl, 6 mg/ml in water), and capromab pendetide (500 μg in 129 μl 0.07 M sodium borate, pH 9.3) was then added. The mixture was incubated at room temperature for 60 min. The conjugate (designated ^{125}I-PIB-capromab) was purified on a NAP-5 column. The purity of the conjugate was determined using ITLC eluted with 80% acetone in water.

For direct iodination, the buffer provided in the commercial kit was changed to 0.1 M PBS, pH 7.5, using a NAP-5 column. For labeling, ^{125}I solution (10 μl, 23 MBq) was mixed with 40 μg capromab in 160 μl PBS. The reaction was initiated by adding 10 μl of chloramine-T solution (2 mg/ml in PBS). After 2 min of incubation at room temperature, the reaction was quenched by the addition of sodium metabisulfite (10 μl, 4 mg/ml in PBS). The conjugate (designated as ^{125}I-capromab) was purified as described above.

For labeling of capromab with iodine-124, 20 μl of [^{124}I]-sodium iodide stock solution was mixed with 4 μl sodium iodide (50 μM in water), and 10 min later 40 μg capromab in 160 μl PBS (prepared as described above) was added. The reaction was performed and the product purified as described above.

In vitro specificity test. PSMA-expressing LNCaP cells were seeded at 10^6 cells per dish in RPMI media or in media designed to induce membrane permeability (Eagle's minimum essential medium, M8167) (25). Experiments were performed 24 h later. All *in vitro* experiments were performed in triplicate.

The cells were washed with PBS and the labeled conjugates added to the cell dishes at concentrations of 10 nM. To saturate the binding sites, a blocking amount of non-labeled capromab (100-fold excess) was added to one set of dishes 15 min before the addition of radiolabeled capromab. Cells were incubated for 2 h at 37˚C. Thereafter, the media was collected; cells were washed once with PBS and detached by treatment with trypsin-EDTA (Biokrom AG). Detached cells were re-suspended and collected. The radioactivity in the samples was measured.

Measurement of immunoreactive fraction. Immunoreactive fraction of radiolabeled conjugates was measured according Lindmo *et al* (28) using cell membranes of LNCaP cells. For unspecific binding cell membranes of PC-3 cells (PSMA nega-

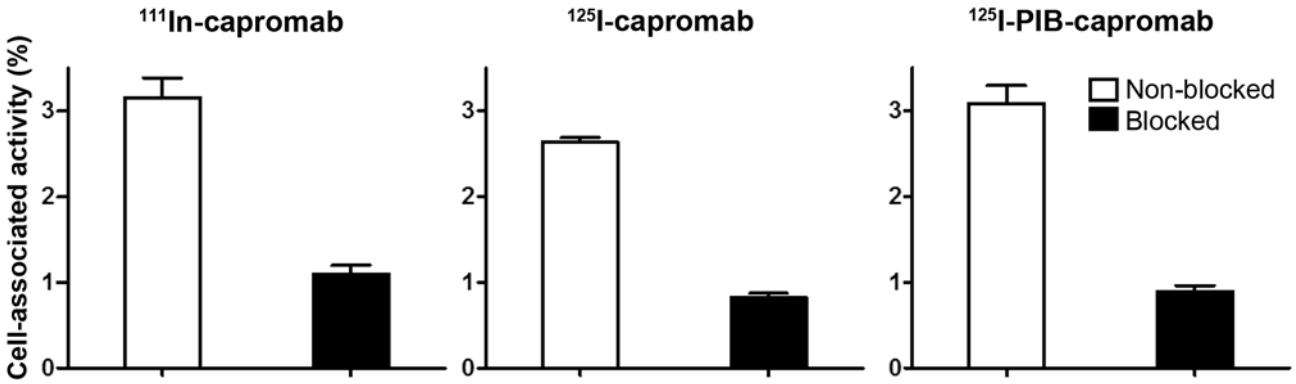

Figure 2. Cell-binding specificity of ^{111}In-capromab pendetide, ^{125}I-PIB-capromab and ^{125}I-capromab. The test was performed using the prostate cancer cell line LNCaP, which was permeabilized to provide access to the intracellular domain of PSMA. In the blocking experiment, binding sites were saturated by adding an excess of non-labeled capromab to the cells. Data are presented as the mean values for three samples ± SD.

tive) were used. The binding assay was set up using 10 nM concentration of labeled antibody and performed at 4˚C. Serial dilution of cell membrane suspension in PBS, starting at 10^7 cells/ml lyzed by Polytron PT 3000 (Kinematica AB, Bohemia, NY), was used. After incubation cell membranes were pelleted and half of the supernatant volume was transferred to Eppendorf tubes. The radioactivity of the samples was measured and the cell associated radioactivity was calculated as $A_{cells} = (A_{pellet + media} - A_{media})/(A_{pellet + media} + A_{media})$. The unspecific binding to membranes of PC-3 cells for each data point was subtracted. The data were plotted as double inverse plot of the applied radioactivity ($A_{pellet + media} + A_{media}$) over the specifically bound radioactivity as a function of the inverse cell concentration (ml/million cells), Fig. 3B. The immunoreactive fraction (IRF) was calculated as IRF = 1/y(x=0).

Biodistribution experiments. All animal experiments were planned and performed in accordance with national legislation on laboratory animal protection. The studies were approved by the Local Ethics Committee for Animal Research. The drinking water for the mice was supplemented with potassium iodide (1%) to prevent accumulation of radioiodine in organs expressing the Na/I symporter (thyroid, stomach, salivary gland, etc.). In comparative biodistribution studies, non-tumor-bearing male NMRI mice were used. In tumor targeting and imaging experiments, male BALB/c nu/nu mice were used. The tumors were grafted by subcutaneous injection of $6x10^6$ LNCaP cells (Matrigel™/medium, 1/1) or $5x10^6$ PC3 cells onto the right hind legs and were allowed to develop for 3 weeks. In all biodistribution studies, the mice (four animals per group) were intravenously injected (tail vein) with a mixture of ^{111}In-capromab (20 kBq) and ^{125}I-capromab (10 kBq) in 100 μl PBS each. The total injected antibody dose was 3 μg per animal. All injections were tolerated well.

In NMRI mice, the biodistribution of ^{125}I/^{111}In-capromab was measured at 4 h and 1, 2 and 3 days pi. At pre-determined time points, sedated animals were euthanized by heart puncture. Samples were collected from blood, heart, lung, liver, spleen, pancreas, stomach, colon, kidney, salivary glands, thyroid, muscle and bone. The intestines along with their content and the carcasses were also collected. The organs and tissue samples were weighed and their radioactivity was measured. A whole gamma-spectrum of each sample was recorded. The organ uptake values are expressed as per cent of injected dose per gram of tissue (% ID/g), except for the thyroid, intestines and the remaining carcass where values are expressed as % ID per whole sample. A paired t-test was used to determine a significant difference ($p<0.05$) between the distributions of ^{125}I and ^{111}In.

Tumor targeting of capromab (labeled with iodine and indium) was compared in a dual isotope study in LNCaP xenografted male mice at 1, 3, 5 and 7 days pi using the protocol described above. The targeting specificity of radiolabeled capromab was measured in PC3 xenografted mice (PSMA negative model) 3 days pi.

Imaging studies. Two tumor-bearing mice were injected with either ^{124}I-capromab (10 MBq) or ^{111}In-capromab (25 MBq) in 100 μl PBS at 10 μg of protein per animal. At five days pi, the animals were euthanized. The urinary bladder was excised post-mortem to improve image quality. Static whole body tomographical examinations were then performed by either microPET [field-of-view (FOV), 7 cm] or microSPECT (FOV, 8 cm; 75A10 collimators, acquisition over 200-250 keV, 32 projections). The remaining amount of tracer in each animal at the time of imaging was 2.75 MBq (^{124}I-capromab) and 5.5 MBq (^{111}In-capromab). Each animal was examined by CT for anatomical correlation following the PET/SPECT examination.

Results

Labeling chemistry. As expected, radiolabeling using ^{111}In was efficient (yield over 99%, specific radioactivity 2.5 MBq/μg), and the conjugate did not require any additional purification. Direct radioiodination was more efficient (yield 71%, specific radioactivity 0.41 MBq/μg) than indirect radioiodination (yield 56%, specific radioactivity 0.017 MBq/μg) for iodine-125. The direct labeling with iodine-124 provided 93% yield (specific radioactivity 1.25 MBq/μg). A simple purification of radioiodinated capromab using a disposable NAP-5 column provided purity of over 99% for all used methods and radioisotopes.

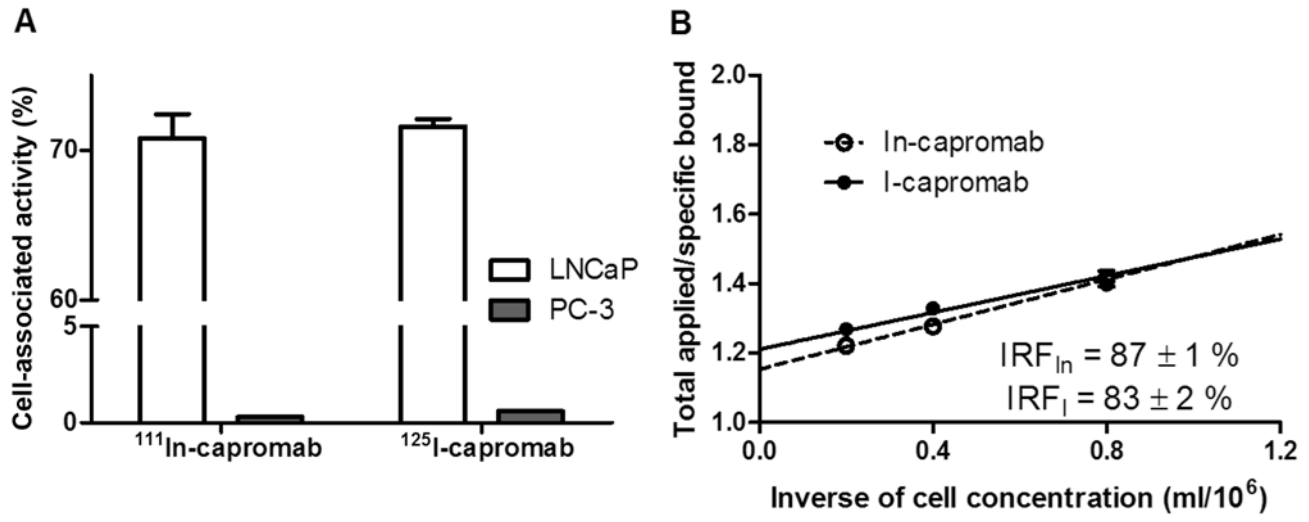

Figure 3. (A) Specificity. Binding of ^{111}In-capromab and ^{125}I-capromab to LNCaP (PSMA-positive) and PC-3 (PSMA-negative) cell membranes. Binding data represent the data point of 0.8 ml/10^6 cells. (B) Immunoreactive fraction. Double inverse plot of the applied radioactivity over the specifically bound radioactivity as a function of the inverse cell concentration for ^{111}In-capromab pendetide and ^{125}I-capromab on LNCaP cell membranes. PC-3 cell membranes (PSMA negative) were used for determination of unspecific binding. The immunoreactive fraction was calculated as 1/y(x=0). Data are presented as mean values corrected on unspecific binding of three samples ± SD. Error bars might not be seen because they are smaller than the point symbols.

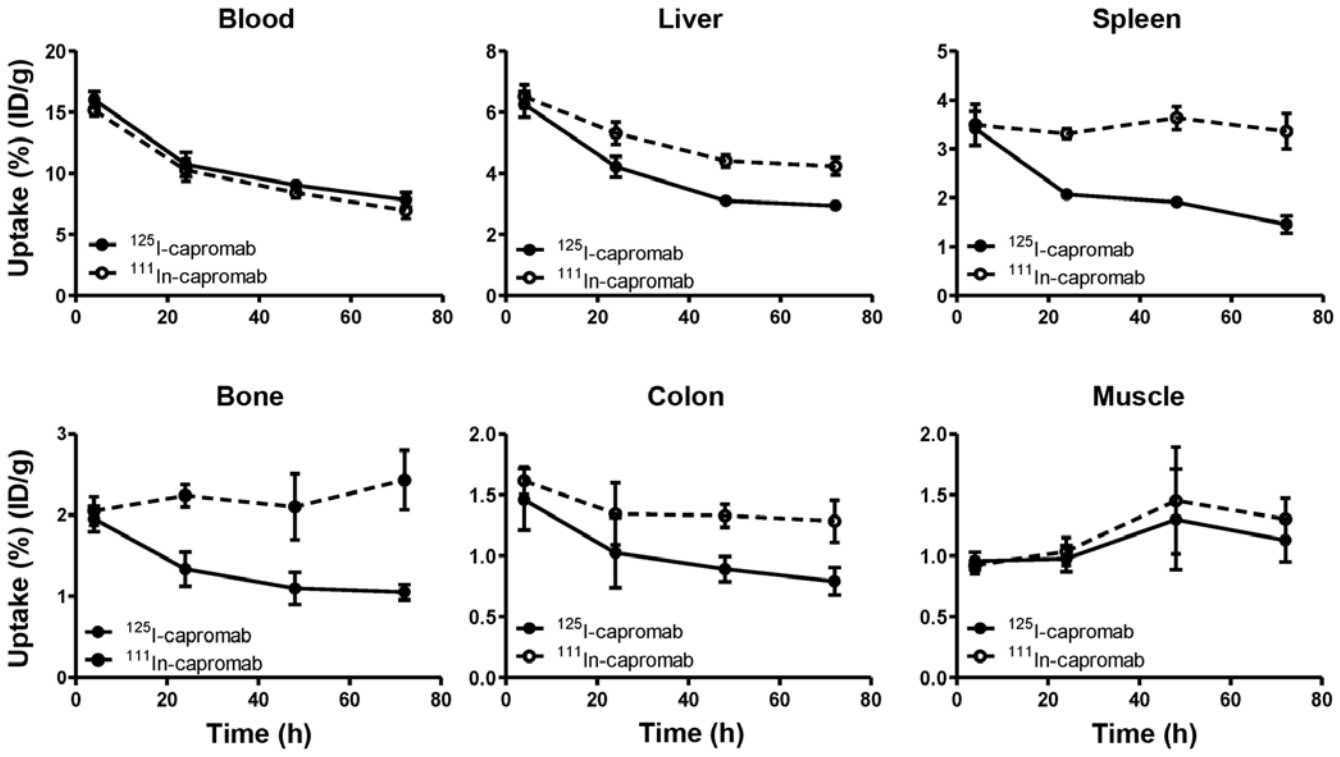

Figure 4. Comparison of the kinetics of ^{125}I-capromab and ^{111}In-capromab in blood and healthy organs in lower abdomen.

In vitro specificity test and immunoreactive fraction. The specificity tests demonstrated that the binding of ^{111}In-capromab, ^{125}I-capromab, and ^{125}I-PIB-capromab conjugates to PSMA-expressing cells was specific because saturation of the binding sites by pre-incubation with non-labeled capromab significantly decreased the binding of the radiolabeled conjugates ($p<0.0001$ for all experiments) (Fig. 2).

Unspecific binding of ^{111}In- and ^{125}I-capromab (Fig. 3A) to membranes of PSMA negative PC-3 cells was 0.4 and 0.8% from binding to membranes from equal amount of PSMA-positive LNCaP cells, respectively. Immunoreactive fraction after labeling was retained (Fig. 3B) and was in the same range for indium-111 (87±1%) and iodine-125 (83±2%) labeled antibody.

Table I. Comparative biodistribution of ^{125}I-capromab and ^{111}In-capromab in male NMRI mice after intravenous injection.

	4 h		24 h		48 h		72 h	
	^{125}I-capromab	^{111}In-capromab	^{125}I-capromab	^{111}In-capromab	^{125}I-capromab	^{111}In-capromab	^{125}I-capromab	^{111}In-capromab
Uptake, %ID/g								
Blood	16.0±0.7[a]	15.2±0.5	10.7±1.0[a]	10.3±0.9	9.0±0.5[a]	8.4±0.4	7.8±0.6[a]	6.9±0.7
Heart	4.3±0.4	4.3±0.3	2.4±0.3	2.7±0.3[a]	2.53±0.05	2.8±0.1[a]	2.09±0.47	2.4±0.5[a]
Lung	5.0±0.6[a]	4.6±0.5	4.2±0.8	4.2±0.6	3.6±0.5	3.9±0.7	3.1±0.3	3.3±0.3[a]
Liver	6.3±0.4	6.5±0.4[a]	4.2±0.3	5.3±0.4[a]	3.1±0.1	4.4±0.2[a]	2.9±0.2	4.2±0.3[a]
Spleen	3.4±0.3	3.5±0.4	2.07±0.05	3.3±0.1[a]	1.9±0.1	3.6±0.2[a]	1.5±0.2	3.4±0.4[a]
Pancreas	1.5±0.4	1.5±0.4	1.4±0.2	1.6±0.3[a]	1.04±0.09	1.4±0.2[a]	1.06±0.09	1.5±0.2[a]
Stomach	1.6±0.2[a]	1.3±0.2	0.9±0.1	1.1±0.1[a]	0.91±0.03	1.2±0.1[a]	0.85±0.12	1.3±0.2[a]
Colon	1.5±0.3	1.6±0.1	1.0±0.3	1.3±0.3[a]	0.9±0.1	1.3±0.1[a]	0.8±0.1	1.3±0.2[a]
Kidney	4.7±0.4	5.3±0.3[a]	2.5±0.3	5.7±0.3[a]	2.3±0.1	7.6±0.7[a]	1.8±0.6	8.1±0.6[a]
Muscle	0.96±0.07	0.92±0.07	0.98±0.11	1.0±0.1[a]	1.30±0.41	1.5±0.4[a]	1.13±0.18	1.3±0.2[a]
Bone	2.0±0.2	2.1±0.2[a]	1.3±0.2	2.2±0.1[a]	1.1±0.2	2.1±0.4[a]	1.05±0.09	2.4±0.4[a]
Thyroid	0.06±0.002	0.06±0.01	0.03±0.01	0.054±0.009[a]	0.08±0.10	0.09±0.07	0.05±0.03	0.09±0.04
GI tract	3.8±0.6	3.9±0.7	2.4±0.6	3.3±0.7[a]	2.1±0.4	3.0±0.5[a]	1.8±0.4	3.3±0.5[a]
Carcass	28±3	30±3[a]	33.9±0.9	40±1[a]	31.9±0.5	40.1±0.6[a]	30±2	40±2[a]

Uptake is expressed as % ID/g and presented as an average value for 4 animals ± SD. Data for the thyroid, gastrointestinal (GI) tract with content and carcass are presented as % of injected dose per whole sample. [a]Uptake of radioactivity was significantly higher than that of the counterpart.

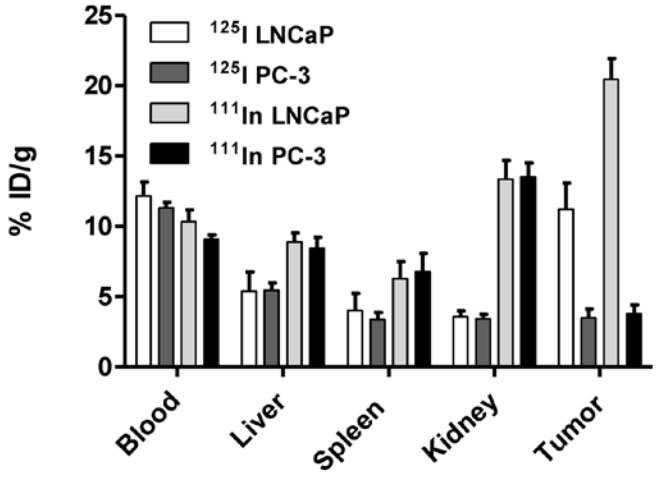

Figure 5. *In vivo* targeting specificity of ^{111}In-capromab pendetide and ^{125}I-capromab in PSMA-positive (LNCaP) and PSMA-negative (PC3) xenografted Balb/c nu/nu male mice 3 days pi.

In vivo experiments. Data regarding the biodistribution of the radiolabeled antibodies in NMRI male mice are presented in Fig. 4 and Table I. The results of the biodistribution experiments suggest that the use of the radioiodine label for capromab results in less accumulation of radioactivity in a number of organs in comparison with the radiometal label. In the lower abdomen, the accumulation of ^{125}I was 1.6-fold lower in colon and 2.3-fold lower in bone in comparison with ^{111}In. The difference for muscle was not as pronounced, but the accumulation of radioiodine was 12% lower, and the difference was significant ($p<0.005$).

In vivo targeting specificity was confirmed in comparison of tumor uptake of radiolabeled capromab in PSMA positive (LNCaP) and negative (PC3) xenografts 3 days pi (Fig. 5). Significantly lower radioactivity uptake was found in PC3 xenografts in comparison with LNCaP xenografts for both ^{111}In-capromab and ^{125}I-capromab ($p<0.01$). There was no significant difference in the uptake by normal organs in mice bearing PC3 and LNCaP xenografts.

Data representing the comparative biodistribution over time in Balb/c nu/nu male mice bearing LNCaP xenografts are presented in Fig. 6 and Table II. In agreement with the biodistribution of radiolabeled capromab in NMRI mice, the concentration of radioactivity in the blood was significantly higher for iodine-125 at all studied time points. Conversely, the accumulation of radioactivity in tumors was lower for the iodinated antibody. In the excretory organs (liver, kidneys, gastrointestinal tract) and organs of low abdomen (colon), the concentration of radioactivity was significantly higher for ^{111}In-capromab. The whole body clearance was more rapid for ^{125}I-capromab.

MicroPET and microSPECT images of mice bearing LNCaP xenografts 5 days pi of ^{124}I-capromab or ^{111}In-capromab are presented in Fig. 7. In both cases tumors were clearly visible. At the same time, the accumulation of radioactivity in the heart and liver was appreciably lower for the iodinated antibody.

Discussion

The sensitivity of radionuclide molecular imaging depends on the contrast. The contrast is dependent on the ratio of the radioactivity concentration in tumors to that in healthy tissues. To obtain maximal contrast, the tumor uptake should be increased and/or the uptake in normal tissues should be decreased as much as possible. In this study, contrast maximization was pursued by minimization of the accumulation in normal tissues. Radioiodine provides the lowest level of radioactivity accumulation in normal organs due to the non-residualizing properties of its radiocatabolites. However, if the radioiodine is attached to an antibody targeting an extracellular antigen present on cancer cells, the same effect is observed in the tumor. In this case, there is no gain in the tumor-to-non-tumor ratio, just a decrease in the signal from tumor. However, capromab binds to the intracellular domain of PSMA. For this reason, it can target only necrotic cells with disrupted membranes. This property was used recently by Ruggiero *et al* (23) in their study monitoring the response to therapy of LNCaP xenografts in a murine model with

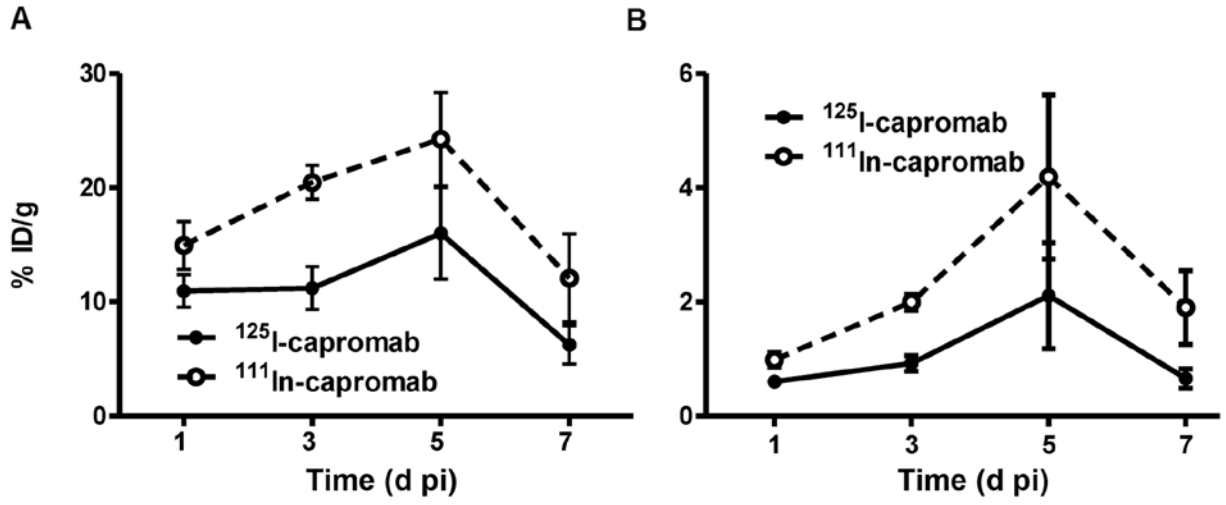

Figure 6. (A) Tumor uptake and (B) tumor-to-blood ratio over time after injection of ^{125}I-capromab and ^{111}In-capromab pendetide in LNCaP xenografted mice.

Table II. Tumor targeting and comparative biodistribution of ^{125}I-capromab and ^{111}In-capromab in male Balb/c nu/nu mice bearing LNCaP xenografts after intravenous injection.

	24 h		72 h		120 h		168 h	
	^{125}I-capromab	^{111}In- capromab	^{125}I-capromab	^{111}In- capromab	^{125}I-capromab	^{111}In- capromab	^{125}I-capromab	^{111}In- capromab
Uptake, % ID/g								
Blood	18.1±0.3[a]	15.1±0.3	12±2[a]	10±2	10±3[a]	7±2	9.2±0.7[a]	6.5±0.5
Heart	4.7±0.6[a]	4.0±0.6	2.8±0.7[a]	2.6±0.7	2.5±0.5[a]	2.2±0.5	2.4±0.2[a]	2.1±0.2
Lung	10±2[a]	8±1	6±2	6±1	5±1	5.7±0.8	4.5±0.7	4.6±0.5
Liver	9±2	14±1	5±3	9±1[a]	3.5±0.7	10±2[a]	3.6±0.5	9±2[a]
Spleen	5.6±0.9	8±1[a]	4±2	6±2[a]	3±2	8±2[a]	3.5±0.4	6.6±0.6[a]
Pancreas	2.0±0.2[a]	1.8±0.2	1.7±0.4	1.8±0.4[a]	1.4±0.5	1.7±0.4[a]	1.1±0.2	1.4±0.2[a]
Stomach	2.6±0.2[a]	1.7±0.2	2.0±0.3[a]	1.49±0.07	1.7±0.3	1.4±0.2	1.4±0.1	1.26±0.10
Colon	2.36±0.06	2.3±0.2	1.4±0.5	1.8±0.6[a]	1.6±0.5	2.1±0.5[a]	1.4±0.2	1.9±0.1[a]
Kidney	5.1±0.1	11.0±0.8[a]	3.6±0.8	13±3[a]	2.6±0.4	14±2[a]	2.5±0.4	15±2[a]
Tumor	11±2	15±4	11±4	20±3[a]	13±8	21±9[a]	6±3	12±8[a]
Muscle	2.3±0.2[a]	1.9±0.2	1.5±0.4	1.5±0.2	1.6±0.5	1.4±0.4	1.3±0.2	1.4±0.2
Bone	2.8±0.1	3.3±0.2	3±1	3.5±0.6	3±1	3.6±0.5	2.3±0.6	3.0±0.7
Thyroid	0.06±0.02	0.05±0.02	0.05±0.02	0.04±0.01	0.04±0.01	0.03±0.01	0.03±0.01	0.02±0.01
GI tract	3.0±0.3	3.5±0.5[a]	2.0±0.3	2.8±0.6[a]	1.4±0.4	2.4±0.5[a]	1.4±0.2	2.7±0.4[a]
Carcass	38±2	39.2±0.7	27±5	32±3[a]	22±5	28±5[a]	20±3	28±2[a]
Tumor-to-organ ratio								
Blood	0.6±0.1	1.0±0.2	0.9±0.3	2.0±0.3[a]	2±2	4±2[a]	0.7±0.3	2±1
Liver	1.4±0.6	1.1±0.2	2.4±0.8	2.3±0.3	5±3	2±2	1.6±0.8	1.4±0.9
Spleen	2.0±0.6	1.9±0.8	3±2	4±1	6±4	3±2	1.7±0.8	1.3±1.0
Pancreas	5±1	8±1	7±3	12±2[a]	14±9	14±8	6±3	8±6
Stomach	4.1±0.7	9±1[a]	6±3	14±2[a]	10±4	16±8	4±2	9±6
Colon	4.6±1.0	7±1	8±3	12±3	12±7	11±6	5±2	6±4
Kidney	2.1±0.5	1.3±0.2	3±1[a]	1.6±0.5	7±3	1.5±0.7	3±1[a]	0.9±0.6
Muscle	4.8±0.7	8±2	8±3	14±2[a]	13±10	17±12[a]	5±2	9±6
Bone	3.9±0.7	4.5±0.8	4±1	6±2[a]	6±2	6±3	3±1	4±2

Uptake is expressed as % ID/g and presented as an average value for 4 animals ± SD. Data for the thyroid, gastrointestinal (GI) tract with content and carcass are presented as % of injected dose per whole sample. [a]Uptake of radioactivity was significantly higher than that of the counterpart.

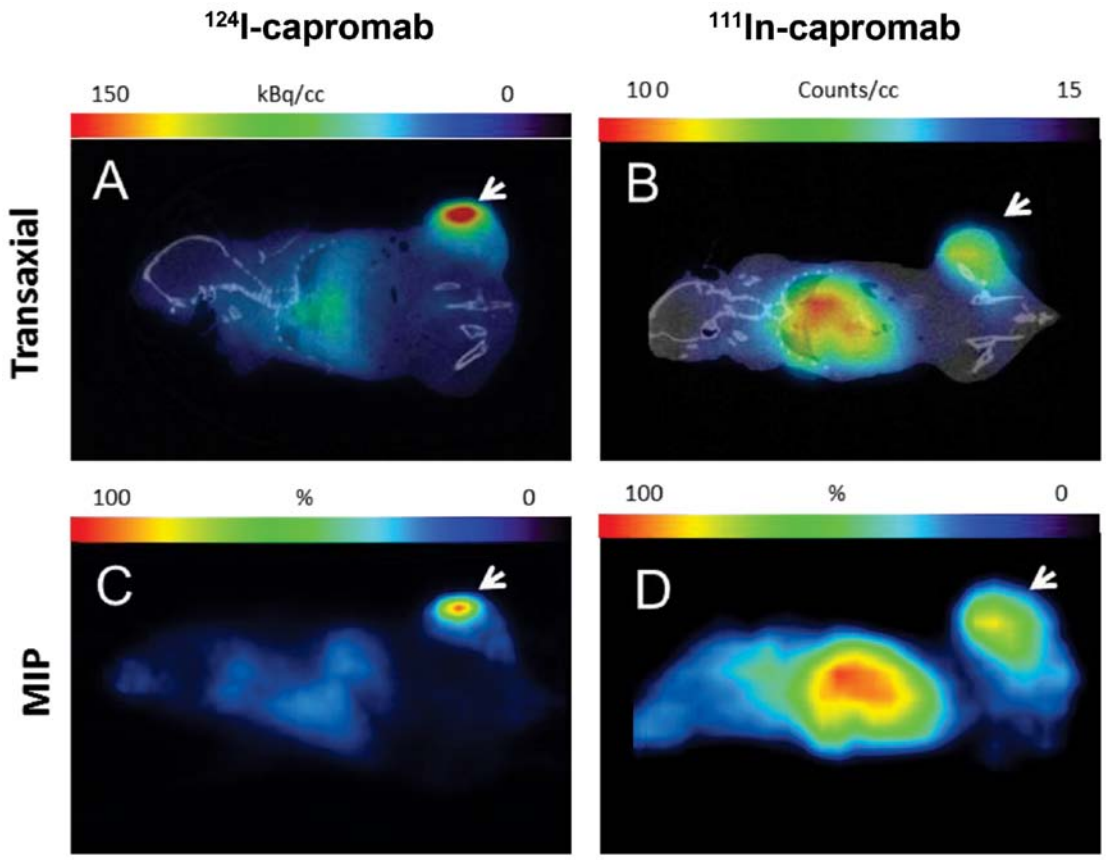

Figure 7. MicroPET/CT and microSPECT/CT images of the uptake of radioactivity in LNCaP xenografts (white arrows) relative to other tissues. Representative transaxial (top panels) and maximum intensity projection (MIP; bottom panels) images of (A and C) ^{124}I-capromab and (B and D) ^{111}In-capromab pendetide-injected mice sacrificed at 5 days post-intravenous injection of 10 MBq ^{124}I-capromab (2.75 MBq/mouse at time of image) or 25 MBq of ^{111}In-capromab pendetide (5.5 MBq/mouse at time of image).

zirconium-89-labeled capromab. They clearly demonstrated that the uptake of radioactivity into tumors irradiated from an external source was as twice as high than that in control tumors due to increased apoptotic and necrotic areas, resulting in cells with disrupted cell membranes. Cellular catabolism is impossible in apoptotic and necrotic cells, and we expected an equal tumor accumulation of radioiodinated and radiometal-labeled capromab.

Our hypothesis was that the tumor uptake would less likely be dependent on the residualizing properties of radiolabel due to the lack of internalization but that clearance from healthy tissues would be improved with the non-residualizing label.

We evaluated two different radioiodination methods, direct radioiodination on tyrosine residues and indirect radioiodination in which the small prosthetic group was radioiodinated and then coupled to lysine groups of capromab. Our results show that direct iodination resulted in an antibody that was as specific for binding to PSMA as that produced by via indirect method. Furthermore, this labeling method did not compromise immunoreactivity of imaging probe that means that imaging contrast should not be decreased due to circulation of non-immunocompetent antibody. Because direct radioiodination is technically simpler, provides higher specific radioactivity, and reduces the probability of user errors, directly iodinated capromab was selected for further evaluation *in vivo*. Use of the directly radioiodinated capromab is a straightforward and practical approach for development of a tracer for prostate cancer staging using immunoPET. The antibody is commercially available, and clinical practice has demonstrated its safety. ^{124}I is also commercially available. Direct radioiodination using chloramine-T is a very robust and reproducible method that could be used to reliably produce large quantities of ^{124}I-capromab. The long half-life of ^{124}I insures that worldwide distribution of ^{124}I-capromab from one or a few production facilities could be feasible. The use of a single facility with well-trained personnel should insure a high quality product.

Biodistribution experiments performed in NMRI mice confirmed our hypothesis that clearance of iodinated capromab from healthy organs of iodinated radiocatabolites is more efficient than that of ^{111}In-capromab (Fig. 4). Concentrations of radioactivity in the liver, spleen and especially bone and colon tissue were significantly higher for the indium-labeled antibody. The concentration of radioactivity in blood was marginally but significantly higher for radioiodine and this difference increased over time, possibly due to the presence of radiocatabolites (28). The uptake of radioiodine in thyroid and stomach, tissues with expressing with Na^+/I^- symporter, was blocked by adding non-radioactive potassium iodide in the drinking water. In humans, the use of Lugol's solution should have similar effect. The radioactivity uptake of radioiodine in

excretory organs (kidneys and liver) was significantly lower than uptake of radioindium throughout the whole experiment. These data support our hypothesis that non-residualizing properties of radioiodine should result in lower uptake of radioactivity in normal organs.

It has been shown for several different antibodies that uptake of ^{111}In and ^{89}Zr in normal organs is very similar, with slightly higher uptake in liver and bones for ^{89}Zr (15,16,18). Comparison of our data for indium-labeled capromab with recently published data for zirconium-labeled capromab showed much higher zirconium concentrations in lung, liver and spleen. Our data regarding biodistribution of the antibody in normal organs and tissues in LNCaP tumor-bearing mice were in good agreement with the data from NMRI mice. The targeting specificity of radiolabeled capromab was confirmed for both conjugates: radioactivity concentrations in PSMA-negative PC3 xenografts were significantly lower (on the level of muscle tissue) than concentrations in PSMA-positive LNCaP xenografts. The tumor uptake and tumor to non-tumor ratios reached maxima at 5 days pi for both labeled conjugates. The tumor uptake of iodinated capromab was significantly lower than that of the indium-labeled antibody, though this difference was not as pronounced as for antibodies and proteins that internalized after binding to extracellular domains of antigens (29-31). For example, tumor-to-blood ratios for ^{111}In- and ^{125}I-labeled trastuzumab, a rapidly internalizing antibody, were at 3 days pi 18±7 and 1.0±0.3, respectively (31). We speculate that the lower radioiodine concentration in tumors might be due to the trapping and processing of capromab by tumor-associated macrophages because reversal of the PSMA intracellular and extracellular domains is impossible.

Despite of the lower tumor concentration of radioiodine, the tumor to non-tumor ratios of radioiodinated capromab were close to that of the indium-labeled antibody throughout the experiment. As we expected, on the day of the image (5 days pi) tumor-to-liver, tumor-to-spleen, and tumor-to-kidney were higher for the non-residualising radioiodine label than for residualising radioindium one. MicroPET/CT and microSPECT/CT imaging of PSMA in mice bearing LNCaP xenografts 5 days pi demonstrated the superiority of the combination of the non-residualizing radioiodine label on the non-internalizing antibody capromab and the PET technique. Radioactivity concentration in liver was much lower in the animal injected with radioiodinated antibody than in the animal injected with radioindium conjugate. LNCaP xenografts visualized with ^{124}I-capromab obviously dominate the image, when xenografts visualized with ^{111}In-capromab had the same intensity as the liver and other tissues in abdomen (where locoregional metastases are expected).

In conclusion, direct radioiodination of capromab provides a targeting agent that binds specifically to living PSMA-expressing cells. Biodistribution of radioiodinated capromab is superior to biodistribution of a radiometal-labeled counterpart due to lower uptake into healthy tissues. Quick clearance of radioiodine from excretory organs together with better resolution of PET vs SPECT can provide higher contrast images of disseminated prostate cancer and improve diagnostic accuracy.

Acknowledgements

This study was supported by grants from the Swedish Cancer Society (Cancerfonden) and the Swedish Research Council (Vetenskapsrådet).

References

1. Takahashi N, Inoue T, Lee J, Yamaguchi T and Shizukuishi K: The roles of PET and PET/CT in the diagnosis and management of prostate cancer. Oncology 2: 226-233, 2007.
2. Lawrentschuk N, Davis ID, Bolton D-M and Scott AM: Positron emission tomography and molecular imaging of the prostate: an update. BJU Int 97: 923-931, 2006.
3. Beresford MJ, Gillatt D, Benson RJ and Ajithkumar T: A systematic review of the role of imaging before salvage radiotherapy for post-prostatectomy biochemical recurrence. Clin Oncol (R Coll Radiol) 22: 46-55, 2010.
4. Schilling D, Schlemmer HP, Wagner PH, *et al*: Histological verification of ^{11}C-choline-positron emission/computed tomography-positive lymph nodes in patients with biochemical failure after treatment for localized prostate cancer. BJU Int 102: 446-451, 2008.
5. Vees H, Buchegger F, Albrecht S, *et al*: ^{18}F-choline and/or ^{11}C-acetate positron emission tomography: detection of residual or progressive subclinical disease at very low prostate-specific antigen values (<1 ng/ml) after radical prostatectomy. BJU Int 99: 1415-1420, 2007.
6. Lilja H, Ulmert D and Vickers AJ: Prostate-specific antigen and prostate cancer: prediction, detection and monitoring. Nat Rev Cancer 8: 268-278, 2008.
7. Raff AB, Gray A and Kast WM: Prostate stem cell antigen: A prospective therapeutic and diagnostic target. Cancer Lett 277: 126-132, 2009.
8. Silver DA, Pellicer I, Fair WR, Heston WD and Cordon-Cardo C: Prostate-specific membrane antigen expression in normal and malignant human tissues. Clin Cancer Res 3: 81-85, 1997.
9. Ulmert D, Evans MJ, Holland JP, *et al*: Imaging androgen receptor signaling with a radiotracer targeting free prostate-specific antigen. Cancer Discov 2: 320-327, 2012.
10. Manyak MJ: Indium-111 capromab pendetide in the management of recurrent prostate cancer. Expert Rev Anticancer Ther 8: 175-181, 2008.
11. Miyamoto DT, Lee RJ, Stott SL, *et al*: Androgen receptor signaling in circulating tumor cells as a marker of hormonally responsive prostate cancer. Cancer Discov 2: 995-1003, 2012.
12. Eder M, Eisenhut M, Babich J and Haberkorn U: PSMA as a target for radiolabelled small molecules. Eur J Nucl Med Mol Imaging 40: 819-823, 2013.
13. Manya MJ, Hinkle GH, Olsen JO, *et al*: Immunoscintigraphy with indium-111-capromab pendetide: evaluation before definitive therapy in patients with prostate cancer. Urology 54: 1058-1063, 1999.
14. Van Dongen GA and Vosjan MJ: Immuno-positron emission tomography: shedding light on clinical antibody therapy. Cancer Biother Radiopharm 25: 375-385, 2010.
15. Brouwers A, Verel I, van Eerd J, *et al*: PET radioimmunoscintigraphy of renal cell cancer using ^{89}Zr-labeled cG250 monoclonal antibody in nude rats. Cancer Biother Radiopharm 19: 155-163, 2004.
16. Nagengast WB, de Vries EG, Hospers GA, *et al*: In vivo VEGF imaging with radiolabeled bevacizumab in a human ovarian tumor xenograft. J Nucl Med 48: 1313-1319, 2007.
17. Perk LR, Stigter-van Walsum M, Visser GW, *et al*: Quantitative PET imaging of Met-expressing human cancer xenografts with ^{89}Zr-labelled monoclonal antibody DN30. Eur J Nucl Med Mol Imaging 35: 1857-1867, 2008.
18. Dijkers EC, Kosterink JG, Rademaker AP, *et al*: Development and characterization of clinical-grade ^{89}Zr-trastuzumab for HER2/neu immunoPET imaging. J Nucl Med 50: 974-981, 2009.
19. Nagengast WB, de Korte MA, Oude Munnink TH, *et al*: ^{89}Zr-bevacizumab PET of early antiangiogenic tumor response to treatment with HSP90 inhibitor NVP-AUY922. J Nucl Med 51: 761-767, 2010.

20. Orlova A, Wållberg H, Stone-Elander S and Tolmachev V: On the selection of a tracer for PET imaging of HER2-expressing tumors: direct comparison of a ^{124}I-labeled affibody molecule and trastuzumab in a murine xenograft model. J Nucl Med 50: 417-425, 2009.
21. Dijkers EC, Oude Munnink TH, Kosterink JG, *et al*: Biodistribution of ^{89}Zr-trastuzumab and PET imaging of HER2-positive lesions in patients with metastatic breast cancer. Clin Pharmacol Ther 87: 586-592, 2010.
22. Divgi CR, Pandit-Taskar N, Jungbluth AA, *et al*: Preoperative characterisation of clear-cell renal carcinoma using iodine-124-labelled antibody chimeric G250 (^{124}I-cG250) and PET in patients with renal masses: a phase I trial. Lancet Oncol 8: 304-310, 2007.
23. Ruggiero A, Holland JP, Hudolin T, *et al*: Targeting the internal epitope of prostate-specific membrane antigen with ^{89}Zr-7E11 immuno-PET. J Nucl Med 52: 1608-1615, 2011.
24. Holland JP, Divilov V, Bander NH, Smith-Jones PM, Larson SM and Lewis JS: ^{89}Zr-DFO-J591 for immunoPET of prostate-specific membrane antigen expression in vivo. J Nucl Med 51: 1293-1300, 2010.
25. Barren RJ III, Holmes EH, Boynton AL, Misrock SL and Murphy GP: Monoclonal antibody 7E11.C5 staining of viable LNCaP cells. Prostate 30: 65-68, 1997.
26. Tolmachev V and Orlova A: Influence of labelling methods on biodistribution and imaging properties of radiolabelled peptides for visualisation of molecular therapeutic targets. Curr Med Chem 17: 2636-2355, 2010.
27. Koziorowski J, Henssen C and Weinreich R: A new convenient route to radioiodinated N-succinimidyl 3- and 4-iodobenzoate, two reagents for iodination of proteins. Appl Radiat Isot 49: 955-959, 1998.
28. Lindmo T, Boven E, Cuttila F, Fedorko J and Bunn PA Jr: Determination of immunoractive fraction of radiolabeled monoclonal antibody by linear extrapolation to binding at infinite antigen excess. J Immunol Methods 72: 77-89, 1984.
29. Khaw BA, Cooney J, Edgington T and Strauss HW: Differences in experimental tumor localization of dual-labeled monoclonal antibody. J Nucl Med 27: 1293-1239, 1986.
30. Meijs WE, Haisma HJ, Klok RP, van Gog FB, Kievit E, Pinedo HM and Herscheid JD: Zirconium-labeled monoclonal antibodies and their distribution in tumor-bearing nude mice. J Nucl Med 38: 112-118, 1997.
31. Malmberg J, Sandström M, Wester K, Tolmachev V and Orlova A: Comparative biodistribution of imaging agents for in vivo molecular profiling of disseminated prostate cancer in mice bearing prostate cancer xenografts: focus on ^{111}In- and ^{125}I-labeled anti-HER2 humanized monoclonal trastuzumab and ABY-025 affibody. Nucl Med Biol 38: 1093-1102, 2011.